ORIGINAL ARTICLE

Photosynthesis supported by a chlorophyll *f*-dependent, entropy-driven uphill energy transfer in *Halomicronema hongdechloris* cells adapted to far-red light

Franz-Josef Schmitt[1] · Züleyha Yenice Campbell[1] · Mai Vi Bui[1] · Anne Hüls[1] · Tatsuya Tomo[2] · Min Chen[3] ·
Eugene G. Maksimov[4] · Suleyman I. Allakhverdiev[5,6,7,8,9] · Thomas Friedrich[1]

Abstract

The phototrophic cyanobacterium *Halomicronema hongdechloris* shows far-red light-induced accumulation of chlorophyll (Chl) *f*, but the involvement of the pigment in photosynthetic energy harvesting by photosystem (PS) II is controversially discussed. While *H. hongdechloris* contains negligible amounts of Chl *f* in white-light culture conditions, the ratio of Chl *f* to Chl *a* is reversibly changed up to 1:8 under illumination with far-red light (720–730 nm). We performed UV–Vis absorption spectroscopy, time-integrated and time-resolved fluorescence spectroscopy for the calculation of decay-associated spectra (DAS) to determine excitation energy transfer (EET) processes between photosynthetic pigments in intact *H. hongdechloris* filaments. In cells grown under white light, highly efficient EET occurs from phycobilisomes (PBSs) to Chl *a* with an apparent time constant of about 100 ps. Charge separation occurs with a typical apparent time constant of 200–300 ps from Chl *a*. After 3–4 days of growth under far-red light, robust Chl *f* content was observed in *H. hongdechloris* and EET from PBSs reached Chl *f* efficiently within 200 ps. It is proposed based on mathematical modeling by rate equation systems for EET between the PBSs and PSII and subsequent electron transfer (ET) that charge separation occurs from Chl *a* and excitation energy is funneled from Chl *f* to Chl *a* via an energetically uphill EET driven by entropy, which is effective because the number of Chl *a* molecules coupled to Chl *f* is at least eight- to tenfold larger than the corresponding number of Chl *f* molecules. The long lifetime of Chl *f* molecules in contact to a tenfold larger pool of Chl *a* molecules allows Chl *f* to act as an intermediate energy storage level, from which the Gibbs free energy difference between Chl *f* and Chl *a* can be overcome by taking advantage from the favorable ratio of degeneracy coefficients, which formally represents a significant entropy gain in the Eyring formulation of the Arrhenius law. Direct evidence for energetically uphill EET and charge separation in PSII upon excitation of Chl *f* via anti-Stokes fluorescence in far-red light-adapted *H. hongdechloris* cells was obtained: Excitation by 720 nm laser light resulted in robust Chl *a* fluorescence at 680 nm that was distinctly temperature-dependent and, notably, increased upon DCMU (3-(3,4-dichlorophenyl)-1,1-dimethylurea) treatment in far-red light-adapted cells. Thus, rather than serving as an excitation energy trap, Chl *f* in far-red light-adapted *H. hongdechloris* cells is directly contributing to oxygenic photosynthesis at PSII.

Keywords *Halomicronema hongdechloris* · Chlorophyll f · Light harvesting · (Uphill) excitation energy transfer · Entropy · Decay-associated spectra

✉ Franz-Josef Schmitt
schmitt@physik.tu-berlin.de

✉ Thomas Friedrich
friedrich@chem.tu-berlin.de

Extended author information available on the last page of the article

Abbreviations

APC	Allophycocyanin
Chl *a*	Chlorophyll *a*
Chl-*a*$_{\mathrm{II}}$	Primary electron donor Chl of PSII (= P680)
Chl *d*	Chlorophyll *d*
Chl *f*	Chlorophyll *f*
DCMU	3-(3,4-Dichlorophenyl)-1,1-dimethylurea
EET	Excitation energy transfer
ET	Electron transfer
FRL	Far-red light (720–730 nm)

LHC	Light-harvesting complex
PBS	Phycobilisome
PBP	Phycobiliprotein
PC	Phycocyanin
Pheo	Pheophytin (primary electron acceptor of PSII)
PQ	Plastoquinone
PSI/II	Photosystem I/II
PsbA	PsbA protein complex (D1 subunit of PSII)
Q_A, Q_B	Primary and secondary plastoquinone molecules in PSII
RC	Reaction center
ROS	Reactive oxygen species
TCSPC	Time-correlated single-photon counting
WL	White light (from white fluorescence bulbs)

Introduction

In photosynthetic organisms, sunlight is absorbed by various light-harvesting complexes. These include chlorophyll-containing membrane-integral light-harvesting complexes (LHCs) in higher plants, large phycobiliprotein (PBP) aggregates (phycobilisomes, PBSs) in cyanobacteria or near-infrared-absorbing bacteriochlorophyll-containing light-harvesting complexes in purple bacteria. Chlorophylls (Chls) are essential molecules for charge separation and electron transfer processes in the reaction centers (RCs) of organisms performing oxygenic photosynthesis. Whereas plants, algae, and cyanobacteria employ Chls *a, b*, and *c*, some cyanobacterial species inhabiting environments of limited light supply or light of certain spectral composition also produce more red-shifted Chl variants, which have been elucidated only recently.

The most abundant chlorophylls, Chl *a, b*, and *c*, have been named in the order of their discovery. The next, more red-shifted, Chl *d*, was discovered as early as 1943 (Manning and Strain 1943), but only decades afterwards, it was unambiguously identified in the cyanobacterium *Acaryochloris marina* (*A. marina*), an organism isolated from a biofilm on the lower side of a didemnid ascidian (Miyashita et al. 1996). Clearly adapted to an ecological niche enriched in far-red and near-infrared light, *A. marina* was shown to contain up to 99% of its total Chl content as Chl *d*, and that Chl *d* can even replace Chl *a* in the photosystems for expanding the active spectrum available to drive oxygenic photosynthesis and carbon fixation to the far-red (Mielke et al. 2011). This has even challenged the paradigm that Chl *a* is indispensable for photosynthetic energy conversion (Allakhverdiev et al. 2010, 2011; Tomo et al. 2011). The name Chl *e* was also given to some pigment long ago (Holt 1966), but neither its chemical nature nor the organism producing it has been identified. While the absorption maximum of Chl *a* in photosystem (PS) II appears at 680 nm, *A. marina* performs light

harvesting with red-shifted antenna Chl *d* with an absorption maximum at 696 nm in methanol and at 714–718 nm for PSII in living cells (Larkum and Kuhl 2005; Marquardt et al. 1997, 2000; Mimuro et al. 1999, 2000, 2004; Miyashita et al. 1996; Schmitt 2011; Schmitt et al. 2006; Theiss et al. 2011).

Recently, the so far most red-shifted chlorophyll named Chl *f* was discovered in a red-light-enriched cyanobacterial culture from stromatolites of Hamelin pool, Australia, which are unique environments for distinct and diverse communities of cyanobacteria (Chen et al. 2010, 2012), and, later, in the cyanobacterial strain KC1 (Akutsu et al. 2011; Itoh et al. 2015). Chl *f* differs from Chl *a* in carrying a formyl group at the C-2 position and is thus determined as [2-formyl]-Chl *a* (Chen et al. 2010; Willows et al. 2013). The optical absorption spectrum of Chl *f* exhibits a red-shifted Q_y transition ($\lambda_{max} = 706$ nm in methanol) compared to the other Chls and a blue-shifted Soret band ($\lambda_{max} = 406$ nm), whereas its maximum fluorescence emission occurs with a remarkably large Stokes shift at 722 nm (in methanol), which is also red-shifted compared to the other Chls (Chen et al. 2010). The latter implies that Chl *f* differs from other chlorophylls by some internal relaxation dynamics like intramolecular vibrational energy redistribution or a solvent/protein-coupled relaxation. Recently, the product of the *psbA4* gene, which is in fact a divergent member of the *psbA* gene family usually encoding D1 core subunits of PSII, has been suggested to work as the Chl *f* synthase (Ho et al. 2016).

The species producing Chl *f* was named *Halomicronema hongdechloris*, and belongs to a cyanobacterial phylum characterized by filamentous growth in the sub-branch of *Leptolyngbya* (Chen et al. 2012). The strategy of *H. hongdechloris* to employ a chemically unique pigment to adapt to far-red light is distinct from the established "red chlorophylls" present in cyanobacteria as well as algae and plants, which are in fact Chl *a* or its multimer states interacting with proteins. The absorption maxima of these red Chl *a* pigments, which are mostly found in light-harvesting complexes (Chen and Blankenship 2011), are shifted up to 740 nm by particular protein-chromophore interactions or Chl-to-Chl excitonic interaction, which modulates the energetic profile (Schlodder et al. 2005). Recently, such adaptive changes resulting in the production of the red-shifted Chl *d* and Chl *f* species have also been observed in several other cyanobacteria in a process termed far-red light photoacclimation (FaRLiP) (Gan et al. 2015). In *H. hongdechloris*, an additional type of complementary chromatic adaptation is operated by remodeling of PBSs under far-red light conditions to employ a special red-shifted allophycocyanin (APC) (Li et al. 2016).

While *H. hongdechloris* cells grown under white light produce only negligible amounts of Chl *f*, the Chl *f*-to-Chl *a* ratio increases reversibly to about 10–12.5% under far-red light (Chen et al. 2012; Li et al. 2014). Similar Chl *f*-to-Chl *a* ratios have recently been found in purified PSI (and PSII)

fractions from far-red light-adapted *H. hongdechloris* cells (Li et al. 2018). Upon cultivation under far-red light, Chl *f* production manifests as a distinct shoulder in the absorption spectrum around 740 nm, and fluorescence emission (at 77 K with 405 nm excitation) exhibits a major peak at 748 nm (Chen et al. 2012). Extensive pigment redistribution occurs in *H. hongdechloris* upon changes in illumination conditions. After transfer from white to far-red light, the PBS content decreases dramatically and PBS undergo extensive remodeling (Li et al. 2016). The authors observed that the fluorescence emission attributed to PBS vanishes almost completely, and also the Chl *a* fluorescence is dramatically reduced.

As it was long the case for Chl *d* in *A. marina*, the role of Chl *f* in photosynthetic energy harvesting by *H. hongdechloris* is still under debate (Allakhverdiev et al. 2016). Nevertheless, Li and coworkers reported that while white light-grown cells did not produce oxygen when illuminated with far-red light, the far-red light-grown cells had still about 50% of the oxygen-evolving activity when far-red light instead of white light was used as sole illumination source, which suggests that Chl *f* is significantly involved in photosynthetic energy harvesting (Li et al. 2014).

Tomo et al. examined fluorescence spectra of *H. hongdechloris* cells grown under white and far-red light at 77 K with a time resolution of about 10 ps. White light-grown cells showed typical fluorescence components for Chl *a* from PSII (685 nm) and PSI (730 nm) immediately upon excitation, with PSII fluorescence decaying mainly with 150 and 520 ps (Tomo et al. 2014). A further red-shifted fluorescence at 742 nm was observed in these cells, which appeared delayed after about 1 ns and was attributed to sensitized emission of a red Chl *a* in one of the photosystems, since Chl *f* is not produced under these conditions. Long-lived ns-fluorescence components at 695, 730, and 742 nm remained indicating energetic equilibration among the Chl *a* pools. In cells grown under far-red light, only a fast decaying (< 10 and 130 ps) 685 nm component and a broad 748 nm fluorescence band with shoulders at 730 nm (attributed to a red Chl *a* of PSI, as above) and 760 nm (attributed to Chl *f*) were observed. The fast 685 nm decay correlated with the rise in 748 nm fluorescence indicating energy transfer from a high energy Chl *a* to Chl *f* and close proximity of these pigments. Since the 748 nm emission persisted with a time constant of more than 10 ns at 77 K, Chl *f* was suggested to represent an energy trap at this temperature (Tomo et al. 2014), although the close proximity of the pigments could indeed favor energy transfer from Chl *f* to Chl *a* at physiological temperatures, as proposed for uphill Chl *d* to Chl *a* energy transfer in *A. marina* (Mimuro et al. 2000). On a faster time scale, energy transfer processes in thylakoid membranes prepared from *H. hongdechloris* cells grown under far-red or white light indicated energy transfer from Chl *a* to Chl *f*,

which appears with a time constant of 1.3 ps along the fastest EET pathway observed at 77 K (Akimoto et al. 2015). It was concluded that equilibration of the Chl *a* and Chl *f* pools at physiological temperature may serve to provide sufficient energy for charge separation by Chl *a* in the RCs; however, the cells would have to carefully regulate the Chl *a*-to-Chl *f* ratio to exclude that excitation energy is trapped on and dissipated by Chl *f* at high Chl *f* contents (Akimoto et al. 2015). In *A. marina*, it is assumed that water oxidation occurs in a heterodimer formed from Chl *a* and Chl *d* (Schlodder et al. 2007), while other groups still propose a RC that is formed by a Chl *a* dimer (Tomo et al. 2007). Since all known oxygenic photosynthetic organisms contain fractions of Chl *a*, this pigment seems necessary to serve as the primary donor in PSII to provide a sufficient redox potential for water oxidation. Thus, the question as to which extent Chl *f* plays a role in photosynthetic energy harvesting is still unresolved.

To investigate EET processes in the living system and under ambient physiological conditions, the present work utilized intact *H. hongdechloris* filaments grown under white light (WL) or adapted to far-red light (FRL) for the measurement of absorption and fluorescence spectra, as well as multichannel time-correlated single-photon counting (TCSPC) at room temperature. Subsequently, decay-associated spectra (DAS) were calculated in order to elucidate pigment-specific fluorescence emission components and to infer possible EET processes. Simulations of the DAS based on systems of rate equations for EET between PBSs, Chl *a* and/or Chl *f* suggest that the ns lifetime of Chl *f*, which would otherwise qualify the pigment as an energy trap, can indeed be an advantage for energy harvesting. However, this is only effective if the Chl *f*-to-Chl *a* ratio does not exceed about 1:10, as seen in vivo under FRL illumination. Under these conditions, the long lifetime of Chl *f* allows the pigment to serve as intermediate energy store for uphill energy transfer to Chl *a* driven by an entropy effect, thereby increasing the efficiency of the photosynthesis reactions under FRL illumination. Direct evidence for an uphill energy transfer in the PSII driven by far-red light excitation of Chl *f* in FRL-adapted *H. hongdechloris* cells based on anti-Stokes fluorescence experiments is presented.

Materials and methods

Cell culture

Halomicronema hongdechloris cultures were kept at room temperature (25 °C) in 50 mL Erlenmeyer flasks containing KES seawater medium under constant shaking, as described (Tomo et al. 2014; Chen et al. 2012) and were grown under white fluorescent light (WL) or far-red light (FRL) by illuminating culture flasks by a circular array of 720 nm LEDs.

Far-red light intensity was adjusted to 10 µE m^{-2} s^{-1}, since at intensities exceeding this value the cultures bleached rapidly due to the reported light sensitivity of the cells, as described (Li et al. 2014). WL intensity was 30 µE m^{-2} s^{-1}.

Absorption spectra

Absorption spectra were recorded on methanolic total pigment extracts freshly prepared from intact WL or FRL-adapted *H. hongdechloris* filament bundles in a 1-cm Quartz cuvette between 270 and 800 nm with UV-1800 spectrophotometer (Shimadzu, Berlin, Germany) at room temperature. The fractions of Chl *a* and Chl *f* were determined from the spectra as the amplitudes from Gaussian fits of the Qy transition bands at 665 nm (Chl *a*) and 707 nm (Chl *f*) based on the respective extinction coefficients of the pigments in methanol (Li et al. 2012).

Fluorescence emission and excitation spectra

Fluorescence emission and excitation spectra were recorded on intact *H. hongdechloris* filaments (see Supplementary Fig. 1) at room temperature in KES medium without prior homogenization. For this purpose, cell colonies were placed directly in the middle of a 1-cm quartz glass cuvette with 1 mm optical path length. The cells were placed inside the excitation light beam and adjusted to maximize the fluorescence signal. The fluorescence and excitation spectra were measured with a Fluoromax-2 spectrofluorometer and corrected for the spectrophotometer's spectral sensitivity with a reference curve provided by the manufacturer (Horiba Jobin Yvon, Bensheim, Germany). The cell filaments were excited at different wavelengths (405–630 nm) using a Xenon lamp (Osram XBO 100, Carl Zeiss, Germany) as light source and wavelength selection with a monochromator, while emission spectra were recorded from 600 to 800 nm at room temperature. Slits were set to 4 nm for excitation and 4 nm for emission, while the integration time was 1 s and the increment 1 nm. Excitation spectra were recorded observing the fluorescence at 650, 686, 715, 739, and 745 nm from 400 up to 5 nm below the corresponding observation wavelength. The light intensity for excitation was about 10 Wm^{-2} on the surface of the filaments and measurement time was 200 s. Since the filaments scatter strongly, the monitored fluorescence might result from areas with local excitation intensity lower than 10 W m^{-2}.

Multichannel time-correlated single-photon counting (TCSPC) and decay-associated spectra (DAS)

Spectrally resolved fluorescence decay curves were recorded on intact *H. hongdechloris* filament bundles at room temperature in KES medium without prior homogenization. For this purpose, cell colonies were transferred into the ca. 1-mm-diameter tip of a Pasteur pipet, which served as spectroscopic cuvette and was placed in a special holder of the multichannel TCSPC setup. Measurements were performed employing a Hamamatsu R5900 16-channel multi-anode photomultiplier tube (PMT) with 16 separate output (anode) elements and a common cathode and dynode system (PML-16C, Becker&Hickl, Berlin, Germany). The polychromator was equipped with a 300 grooves/mm grating resulting in a spectral resolution of the PML-16C of 12.5 nm/channel. A 632 nm pulsed laser diode (PDL-600, Becker&Hickl, Berlin) delivering 80 ps FWHM pulses, driven at a repetition rate of 20 MHz, was used for excitation. The fluorescence was observed via a 632 nm longpass filter (F76-631, AHF Analysentechnik, Tübingen, Germany). The laser intensity for excitation was 80 Wm^{-2} on the surface of the filaments and measurement time for each time-resolved study was 300 s. Since the filaments scatter strongly, the monitored fluorescence might result from areas with lower excitation intensity than 80 Wm^{-2}.

To determine DAS, the fluorescence decays were analyzed employing a Levenberg–Marquardt algorithm for the minimization of the reduced $\chi_r^2(\lambda)$ in each wavelength segment. The influence of the instrumental response function (IRF), which is the registered response to scattered laser pulses, is considered during that fitting procedure as the determined exponential decay with three exponential components is convoluted with the IRF before comparison with the measured data and the calculation of $\chi_r^2(\lambda)$ and averaged over all time channels as described in (Schmitt 2011). The multiexponential fits of all decay curves measured in one time- and wavelength-resolved fluorescence spectrum were performed as global fits with common values of lifetimes τ_j for all decay curves (linked parameters) and wavelength-dependent pre-exponential factors $a_j(\lambda)$ (non-linked parameters). The result of this analysis is usually plotted as a graph of $a_j(\lambda)$ for all wavelength-independent lifetimes τ_j, representing so-called normalized decay-associated spectra (DAS) that reveal the spectral distribution of individual decay components. For this calculation, the software of Globals Unlimited (University of Illinois, Urbana, USA) was used. Each symbol in the DAS represents the results in the corresponding wavelength channel. The symbols are connected by a spline function to guide the eye.

Anti-Stokes fluorescence measurements

Intact *H. hongdechloris* filament bundles were transferred into a spectroscopic quartz cuvette (1 mm path length) filled with KES medium and placed in a Peltier-controlled cuvette holder Qpod 2e (Quantum Northwest, USA) that allowed to stabilize temperature between 0 and 40 °C. After

adjusting the cell bundle in the cuvette to the laser beam, Chl *f* was excited using a ps-pulsed white light supercontinuum laser (Fianium Ltd., UK) via a 720 ± 10 nm bandpass filter (FB720-10, Thorlabs, Germany) to select for the excitation light and a 680 ± 10 nm bandpass filter (FB680-10, Thorlabs, Germany) to select for blue-shifted anti-Stokes fluorescence emission. A single-photon avalanche photodiode (SPAD PDM-type, Micro Photon Devices, Milan, Italy) was used as time-resolved fluorescence detection device and a SPC-530 time-correlated single-photon counter (Becker & Hickl, Berlin, Germany) was employed for data acquisition.

Mathematical modeling

The formalism of rate equations can be used treating different molecules as localized states. A simplified model respects the given resolution of the measurement setup employing the concept of "compartments," which could be different light-harvesting complexes or the RC [for details regarding the simulation, see Schmitt (2011)].

The states and the couplings between them are modeled by rate equations subsuming the probabilities per time unit to populate the observed states by EET from donor states, or to depopulate the states by EET to acceptor states, or radiative/non-radiative relaxation into the ground state. This leads to a set of coupled linear 1st order differential equations that can be solved to obtain the excited state dynamics of all involved compartments. The fluorescence intensity is proportional to the time-dependent population density of the fluorescing states that is calculated from the solution of such a set of coupled linear differential equations 1st order. This set of equations is solved by a sum of exponential functions with different time constants. In a non-degenerated set with *n* pair-wise different eigenvalues of the transfer (coefficient) matrix $\bar{\bar{T}}$ describing the change $\dot{\bar{N}}$ of all *n* state population densities, the set of differential equations can be written according to Eq. (1) (Schmitt 2011):

$$\dot{\bar{N}} = \bar{\bar{T}} \bar{N} \tag{1}$$

The solution for the i-th state population density is given by

$$N_i(t) = \sum_{j=1}^{n} U_{ij} e^{\gamma_j t} \tag{2}$$

in which γ_j is denoting the *j*-th eigenvalue and U_{ij} the *i*-th component of the *j*-th eigenvector of $\bar{\bar{T}}$. For a non-degenerated system, Eq. (2) is proportional to the assumed fluorescence decay:

$$F(t, \lambda) = \sum_{i=1}^{n} A_i(\lambda) e^{(-t/\tau_i)} \tag{3}$$

with $\gamma_j = -\left(\tau_j\right)^{-1}$ according to the proportionality between fluorescence intensity and excited state population density. Equation (1) is suitable to calculate the expected fluorescence emission in the time domain from the transfer matrix $\bar{\bar{T}}$. Vice versa, $\bar{\bar{T}}$ can be reconstructed, if the time-resolved fluorescence kinetics of all compartments which are modeled as states is measured. Consequently, the time-dependent fluorescence of emitters described by a coupled system of differential equations as given by Eq. (1) occurs multiexponentially with up to *n* decay components (i.e., exponential decay time constants) for *n* coupled subsystems [i.e., *n* coupled states determine the dimensionality of the transfer matrix to be equal to *n* with respect to Eq. (1)]. By application of this formalism, the decay-associated spectra (DAS) can be simulated for each compartment in a coupled system, if one adds a Gaussian lineshape for the emission spectrum of each compartment that exhibits fluorescence.

Results and discussion

Absorption spectra of total pigment extracts

H. hongdechloris cells previously grown under WL (30 µE m^{-2} s^{-1}) were subsequently illuminated for several days with FRL (720–730 nm) at low intensity (10 µE m^{-2} s^{-1}) and total methanolic extracts were prepared of these samples to analyze changes in the pigment content (Fig. 1). Fluorescence microscopy on *H. hongdechloris* filaments cultivated under WL or transferred to FRL confirmed the typical changes in the cellular pigment distribution (Supplementary Fig. 2), as reported previously (Li et al. 2014; Majumder et al. 2017).

Figure 1 shows the absorption spectra of total methanolic pigment extracts from *H. hongdechloris* cells, which had first been adapted to WL, and were then either continued to be illuminated with WL or transferred to FRL for different time periods. Besides the maximum at 665 nm, which is attributed to the Q$_y$ band of Chl *a* and was used for normalization, the chlorophyll Soret band is localized at 430 nm, but this strongly overlaps with carotenoid absorption between 400 and 500 nm.

The graph shows distinct changes in pigment composition when the cells are grown under FRL in comparison to the WL control sample (Fig. 1A, B). Already after 2 days, a distinct absorption feature with maximum at 707 nm appears and can clearly be seen after 5 days, which was absent in all WL-grown samples, and is attributed to formation of Chl *f*. The relative content of the Chl *f* emission at 707 nm was determined from the area of a Gaussian fit of the Chl *f* emission at 707 nm and compared to a single Gaussian fit of the Q$_y$ absorption band of Chl *a* at 665 nm. The absorption
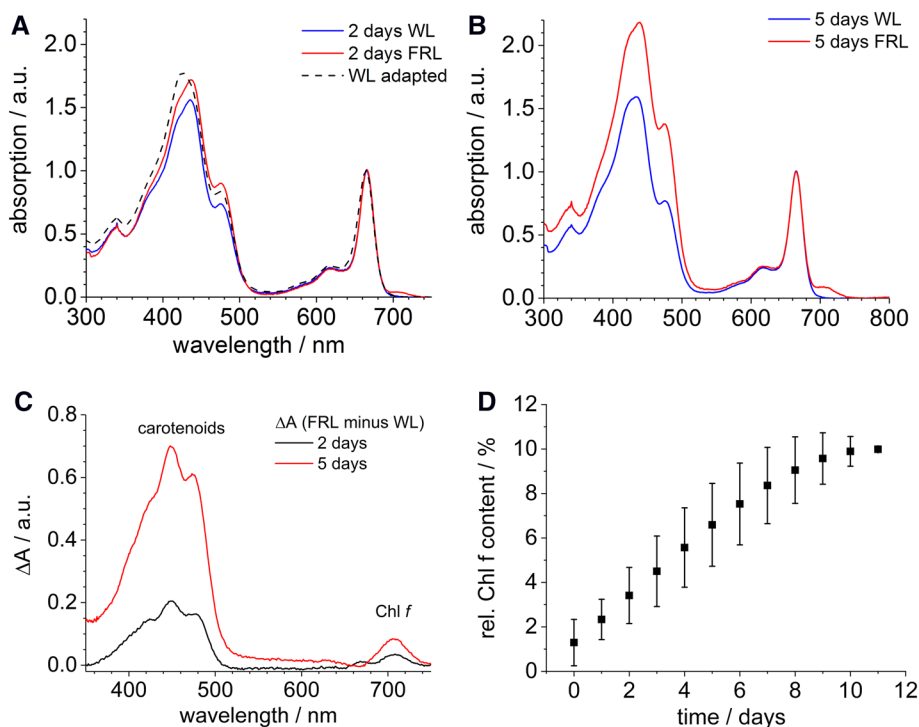
Fig. 1 A Room temperature absorption spectra of methanolic extracts of *H. hongdechloris* cells (i) adapted to WL (dashed) as the initial control sample, (ii) of a sample illuminated with FRL for 2 days (red), and (iii) in comparison to a control sample which was continued to be grown under WL for 2 days (blue). **B** Absorption spectra of *H. hongdechloris* methanol extracts from cells illuminated with FRL for 5 days (red) in comparison to a control sample which was continued to be grown under WL for 5 days (blue). All spectra are normalized to 1 at the Chl *a* absorption peak at 665 nm. **C** Absorption difference spectra of *H. hongdechloris* extracts from cells grown under FRL for 2 and 5 days, respectively, in comparison to the corresponding control sample grown under WL. **D** Relative amplitude of the Chl *f* Q_y absorption band from spectra as in **A** and **B** determined by Gaussian fits of the bands at 707 nm for Chl *f* and at 665 nm for Chl *a*, respectively ($n = 5$)

of Chl *f* rises up to a relative content of 10% compared to Chl *a* after 12 days of FRL illumination (Fig. 1D), but does not seem to grow further (data not shown). Even after three weeks of FRL illumination no stronger absorption at 707 nm was observed. Also in the 400–500 nm range, a distinct increase in absorption can be observed for the FRL samples, which continuously grows, and the corresponding difference spectra (Fig. 1C) strongly resemble the absorption of β-carotene, as noted previously (Chen et al. 2012). When put back to WL of an intensity of 30 µE m^{-2} s^{-1}, the content of Chl *f* started to decline (data not shown). There is some discrepancy between literature data regarding the conditions leading to increased β-carotene content. Li et al. (2016) had found that the β-carotene content of cells adapted over weeks to FRL is larger than in cells grown in WL. However, the previous work by Chen et al. (2010) had shown in Fig. 3D that the β-carotene content increases after transfer of previously FRL-adapted cells into WL for 2 days. Different results determined under different culture conditions indicate that transient changes in β-carotene content may be a general response to changes in light conditions, especially in the first days of re-acclimation. It should be noted that these

methanolic extracts do not reflect the absorption spectra of whole cells, in which, in addition, prominent changes due to redistribution and remodeling of PBS can be observed (Chen et al. 2010, 2012). Of note, since the bilin pigments are covalently attached to the PBPs, they cannot be extracted by organic solvents.

Fluorescence emission and excitation spectra

Figure 2 shows the fluorescence emission spectra of intact *H. hongdechloris* filaments after transfer to FRL illumination. The samples are excited with 580 nm light, which preferentially excites PBS and, therefore, gives rise to PBS fluorescence as well as fluorescence of molecules which are coupled to the PBS via EET. The emission in the 715–740 nm spectral range increases during adaption to FRL. In contrast, samples persistently kept on WL seem to loose fluorescence in the red spectral region, which may be due to a loss in red-shifted PBS. However, strong variations of the ratio of far-red fluorescence (715–740 nm) to PBS fluorescence (650 nm) are observed. After two days under FRL (Fig. 2B), a strong fluorescence band peaking at ~750 nm
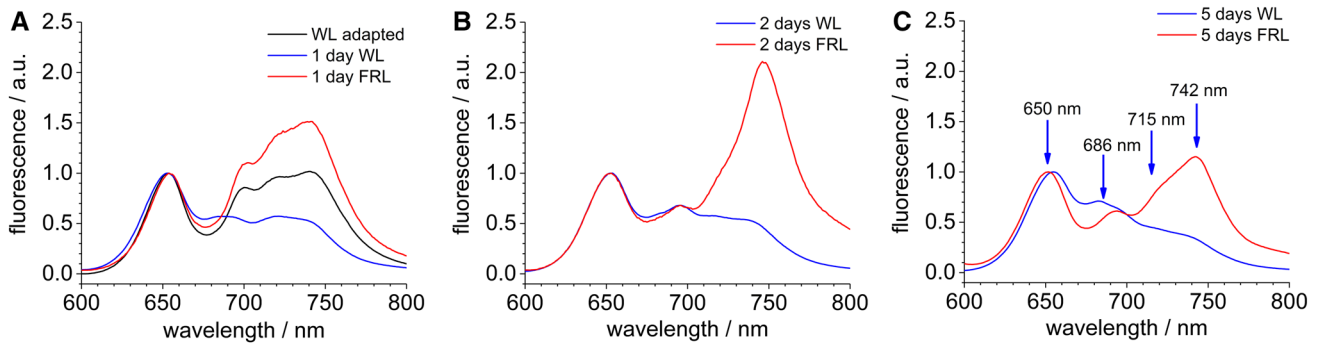
Fig. 2 Room temperature fluorescence spectra of intact WL-adapted *H. hongdechloris* cells upon excitation with 580 nm (black) and for samples subsequently illuminated with WL (blue) or FRL (red) for 1 day (**A**), 2 days (**B**), and 5 days (**C**), respectively. All curves were normalized to unity at 650 nm. Arrows in (**C**) indicate the peak positions of major fluorescence emission bands/shoulders

Fig. 3 Room temperature fluorescence spectra of intact *H. hongdechloris* cells. Samples that had been adapted to WL were subsequently illuminated with FRL for several days, as indicated, and fluorescence was excited with 405 nm (**A**) and 470 nm (**B**), respectively. All curves were normalized to unity at 680 nm. **C** Time course of the 739 nm peak fluorescence during FRL adaptation (excitation with 470 nm, $n=5$). Excitation spectra for *H. hongdechloris* cells adapted to WL (**D**) or to FRL for 2 days (**E**) or 5 days (**F**), respectively, monitored at observation wavelengths 650, 686, 715, 739, and 745 nm
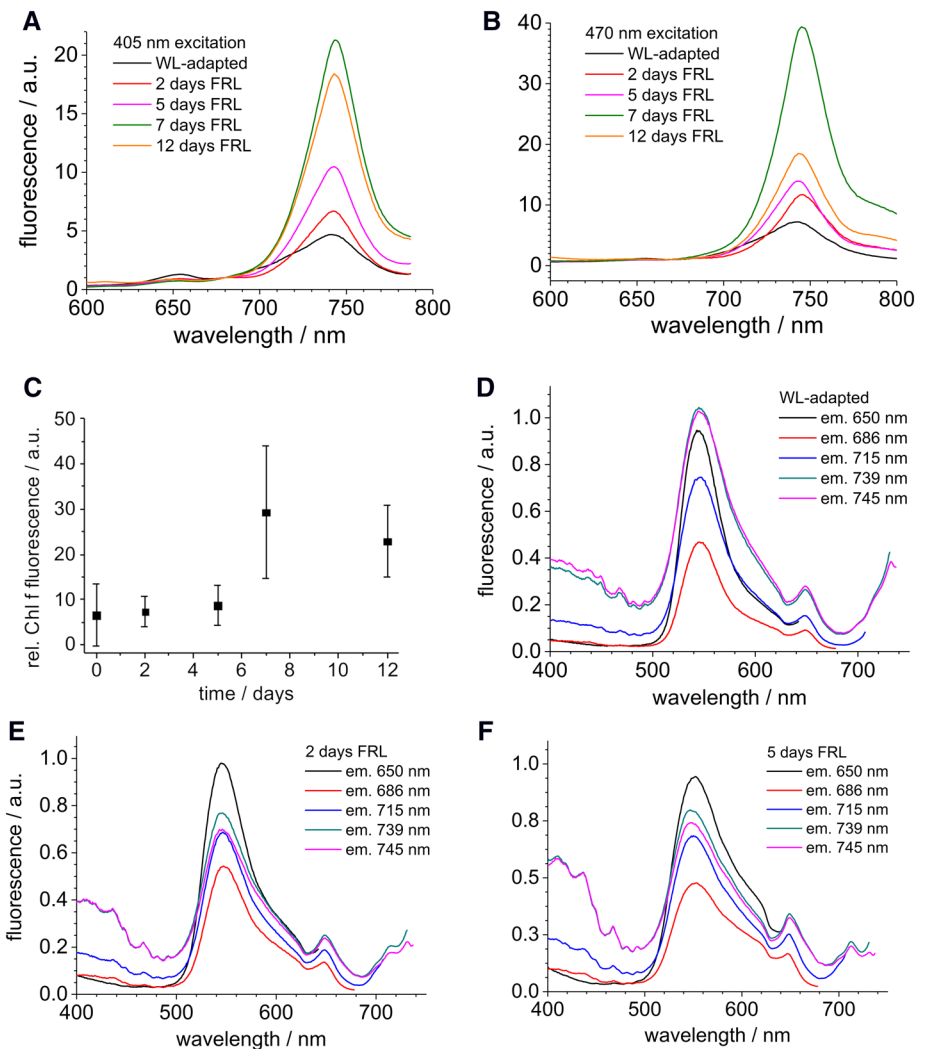
occurs, which apparently has a shoulder at ~720 nm. The 750 nm central peak can be attributed to Chl *f* fluorescence, in line with previous observations (Chen et al. 2012). The presence of fluorescence at 715–740 nm in WL-adapted cells, in which no Chl *f* was detected (Chen et al. 2012), suggests that the emission strongly overlaps with far-red-shifted PBS and red Chl *a*. The strong Chl *f* emission already indicates that it might be sensitized emission due to energy

transfer from PBS absorbing at 580 nm. There are indications that the Chl *f* fluorescence observed after 2 days of FRL illumination is reduced again after longer time periods, as observed previously (Majumder et al. 2017). The fluorescence spectrum of *H. hongdechloris* filaments adapted to FRL over 5 days exhibits major peaks at 742 nm (with a shoulder at 715 nm), 650 nm, and a smaller one at 686 nm (Fig. 2C). Around 650–660 nm, several phycocyanin (PC) and allophycocyanin (APC) species of the PBP antenna are expected to contribute, the region around 750 and 780 nm indicates that more than one species with long-wavelength fluorescence spectrum are present in the regime, which cannot be resolved. The analysis of these species reaches beyond the scope of the present study and will be subject of future analysis. The peak at 650 nm is attributed to PBS emission, the one at 686 nm is attributed to Chl *a* emission, and in the long-wavelength regime at 715 and ~740 nm, the signals are dominated by Chl *f*, low-energy Chl *a* species and red-shifted PBS emission (Majumder et al. 2017; Tomo et al. 2014). This indicates that at least two long-wavelength emitters with remarkably different emission wavelengths at 715 and ~740 nm are involved in the fluorescence spectra of *H. hongdechloris* after 7 days under far-red light.

Figure 3A, B shows fluorescence emission spectra of intact *H. hongdechloris* filaments after illumination with FRL for several days. To analyze the coupling between the PBS and the Chl-containing membrane protein complexes, fluorescence emission was recorded upon excitation with 405 nm (Fig. 3A), which excites Chl *a* and Chl *f*, and with 470 nm (Fig. 3B), which preferentially excites Chl *f* (Niedzwiedzki et al. 2014; Chen 2014). Again, a quantitative comparison of the spectra is difficult due to the variant intensities of the live-cell samples. Therefore, the fluorescence intensity at 680 nm was used for normalization of the spectra, because this is close to the Chl *a* emission peak and Chl *a* is the most stable pigment according to previous publications. The fluorescence spectra excited with 470 nm (targeting Chl *f* and Chl *a*) show a strong increase of the fluorescence of Chl *f* and possible further red PBS or Chl species at 740–750 nm after 5 days of FRL illumination (Fig. 3B) possibly followed by a slight decline, but, additionally, large variations for longer FRL illumination times occur (Fig. 3C).

To get more insight into the involved species, which were resolved at 715 and around 739 nm (see Fig. 2C), we added a series of fluorescence excitation experiments to compare WL-adapted samples (Fig. 3D) with cells grown under FRL for 2 or 5 days (Fig. 3E, F). The results show that there is far-red emission also in WL-adapted cells, which is mainly excited at 550 nm and accordingly attributed to the absorption of PBS. This especially accounts for the observed emission at 739 and 745 nm. However, for WL-adapted cells (Fig. 3D), the fluorescence at 715, 739, and 745 nm has only small excitation amplitude between 400 and 450 nm.

Therefore, we conclude that it is not possible to excite the far-red fluorescence via the Soret band of chlorophylls, but mainly via the absorption of PBS. Thus, we propose that the far-red species in WL-adapted samples mainly result from red-shifted PBS, in particular red-shifted APC, as suggested by (Li et al. 2016). The situation is different after 2 and 5 days of FRL acclimation (Fig. 3E, F), when pronounced excitation of the far-red emission at 739 and 745 nm is also observed between 400 and 450 nm indicating that the Soret band of chlorophylls contributes to the excitation of far-red fluorescence. These findings suggest that in WL-adapted cells, mainly red-shifted PBS contribute to the far-red emission, while after FRL adaption, Chl *f* (or possibly additional red-shifted Chl *a*) is formed and accordingly contributes to the far-red emission.

The fluorescence excitation spectra additionally indicate energetic coupling between the involved pigments. Figure 3D indicates that the far-red emission (at 739 and 745 nm detection wavelength) is most efficiently excited at 550 nm, i.e., the region of PC. In addition, there is an excitation band at 660 nm (APC or Chl *a*) and increasing excitation in the red at 715 nm, where direct excitation of red-shifted APC occurs (Li et al. 2016). The strong excitation band at 550 nm indicates that EET from PC to red-shifted APC is intact (Li et al. 2016). After 2 and 5 days of FRL adaption (Fig. 3E, F) the far-red emission bands at 715, 739, and 745 nm are still preferentially excited at 550 nm indicating that the functional EET from PC to the red-shifted molecules in the antenna complexes is still active. The excitation of fluorescence at 739 and 745 nm shows an additional local maximum around 710 nm after 5 days of FRL adaption indicating the presence of a new species, which most likely is Chl *f*.

These observations suggest that EET at least partially occurs directly from PC and APC in the PBS to Chl *f*. However, functional coupling between different red-emitting species cannot be proven by steady-state spectroscopy. The spectra for the fluorescence excitation of PBS (650 nm) and Chl *a* (686 nm) indicate a maximum of excitation at 550–560 nm with a broad shoulder up to 640 nm, which is attributed to different species of PC and APC molecules. The spectra indicate that all these species are coupled and excited via blue-absorbing PC (550 nm) and further PC and APC species up to 660 nm (Li et al. 2016). To get more insight into the underlying processes, time-resolved fluorescence spectroscopy was performed on intact *H. hongdechloris* cells.

Time-resolved fluorescence spectra and DAS

Decay-associated spectra (DAS) can yield valuable information about the excitation dynamics and EET processes in heterogeneous and possibly coupled chromophore systems.

Using multichannel TCSPC, spectrally resolved fluorescence decays were recorded with 632 nm pulsed excitation on intact filament bundles of *H. hongdechloris* cells, either WL-adapted or after transfer to FRL for 2 or 4 days. Examples of such emission wavelength-dependent fluorescence decay curves are shown in Fig. 4 for two selected emission channels, 660 nm (PBS emission) and 730 nm (red Chl *a* and Chl *f* emission). In WL-adapted cells, PBS emission at 660 nm (Fig. 4A, black curve) is dominated by a fast 115 ps component (see description of the corresponding DAS below, Fig. 4D), whereas fluorescence at 730 nm (red curve) decays predominantly with a 160 ps component, and shows a small rising phase indicative of sensitized emission. In 4-days FRL-adapted cells (Fig. 4B), PBS fluorescence at 660 nm is dominated by a 140 ps decay phase, whereas fluorescence at 730 nm clearly shows a prolonged rising phase, indicating sensitized emission by EET from PBS, and the subsequent decay is dominated by slow components with decay times of 300 ps and 1.1 ns (see description of the corresponding DAS in Fig. 4F). A direct comparison of 730 nm emission from WL- and FRL-adapted cells is shown in Fig. 4C, directly indicating the much slower decay and the slower fluorescence rise kinetics in FRL-adapted cells.

The DAS (Fig. 4D–F) reveal that the fluorescence decays of all samples could consistently be approximated by the sum of three exponential decay components with distinct spectral dependence, a fast (115–140 ps), an intermediate (160–300 ps) and a slow one (750–1100 ps). The DAS of WL-grown cells (Fig. 4D) allow to discriminate three spectral regions, the first around 650 nm, in which mainly PBS fluorescence is observed, the second around 680 nm, mainly attributed to Chl *a* (in PSII) and the third around 730 nm, which contains the phonon side bands (caused by intramolecular vibrations) and possible contributions from low-energy Chl *a* and red-shifted PBS (Li et al. 2016; Majumder et al. 2017). PBS fluorescence at 650 nm is dominated by a fast 115 ps decay component and only minor contributions of a 750 ps decay time, which, from its spectral characteristics, can mainly be attributed to chlorophylls. Notably, the spectrum of the 115 ps component changes sign and exhibits a large negative amplitude peaking at 685 nm. A minor negative amplitude is emerging around 730 nm, which could be due to red Chl *a* molecules present in the photosystems. Since a negative DAS amplitude corresponds to a rising component in the time-resolved fluorescence curve, the temporal correspondence between PBS fluorescence decrease
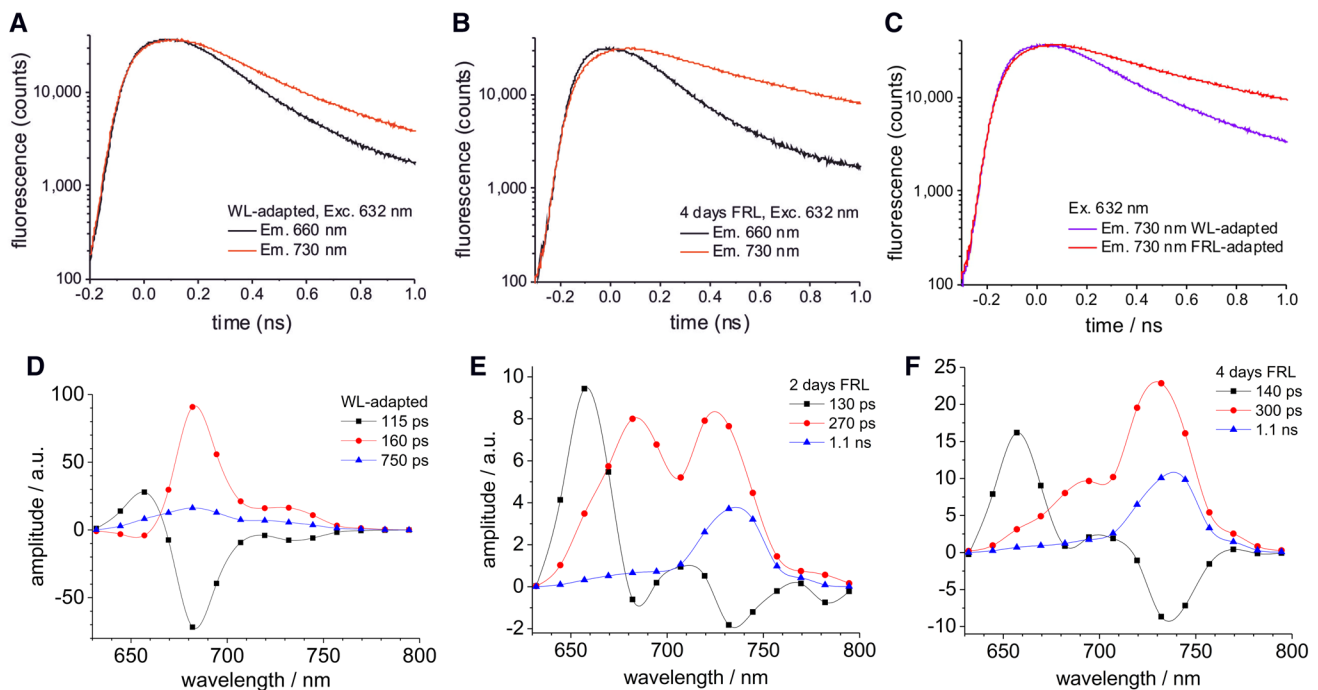

Fig. 4 Examples of spectrally resolved fluorescence decays measured on intact filament bundles of *H. hongdechloris* cells adapted to WL or to FRL for various periods and the resulting decay-associated spectra (DAS) at room temperature. Fluorescence decays in the indicated spectral channels (PBS emission: 660 nm, black; Chl *f* emission: 730 nm, red) measured from WL-adapted cells (**A**) or cells grown for 4 days under FRL (**B**). **C** A direct comparison of 730 nm emission for WL- (purple) and 4 days FRL-adapted cells (red). For calculation of the DAS, three exponential components were necessary to obtain good global fitting results. The DAS correspond to WL-adapted cells (**D**), or to cells grown for 2 (**E**) or 4 days (**F**) under FRL. The spectra of the individual temporal components are indicated by different colors. The superimposed lines are cubic spline curves connecting the data points, which were included to guide the eye

and Chl fluorescence rise demonstrates EET from PBS to Chl molecules of PSII.

The DAS of cells measured 2 days after transfer to FRL (Fig. 4E) showed an intermediary behavior as compared to cells adapted to FRL for 4 days (Fig. 4F). Here, the PBS fluorescence decay around 650 nm is dominated by a large fast 130–140 ps component, but the corresponding negative DAS amplitude around 685 nm has almost completely vanished, and a larger negative amplitude occurs around 730 nm. This indicates that while EET from PBS to Chl a is reduced, an energy transfer to Chl f starts to emerge. The fluorescence around 730 nm is strongly increased and decays mainly with an intermediate 270–300 ps time constant, and a smaller component decaying with 1.1 ns, which is exclusively observed in the 730 nm region, and, thus, identifies this region as Chl f fluorescence.

After 4 days of FRL adaption (Fig. 4F), the contribution from the 680 nm region is largely reduced indicating that PBSs are able to transfer parts of the excitation energy directly to Chl f. This observation is remarkable, since the excitation wavelength used (632 nm) should mainly target PC and APC in normal, but not red-shifted PBSs, which have been shown to undergo spatial segregation from photosystems during FRL adaptation (Li et al. 2014; Majumder et al. 2017). Therefore, it is proposed that re-exposure of FRL-adapted cells to light of wavelengths below 700 nm (by the 632 nm excitation laser) already causes changes in PBS distribution and re-coupling of PBS to photosystems as part of a normal physiological response. The study of such time- and light-dependent processes will be the subject of follow-up work.

Modeling of energy transfer processes

In order to interpret the DAS of WL- and FRL-adapted *H. hongdechloris* cells, the DAS were simulated by setting up rate equation systems for appropriate minimal kinetic models. Since the DAS were all recorded upon excitation with 632 nm in the main PBS absorption band, these models mainly encompass EET processes from PBS to Chl a molecules including those in the RC of PSII, which results in primary charge separation and the production of a radical pair consisting of the chlorophyll special pair and a pheophytin (frequently expressed as $(Chl)_2^{+\cdot}/Pheo^{-\cdot}$, in the following denoted as $Chl^+/Pheo^-$), from which then the electron is transferred further and charge separation is stabilized by transfer to the primary plastoquinone (PQ) Q_a. Figure 5A represents the situation in WL-adapted cells, in which no Chl f is present. EET can occur reversibly between PBS and Chl a, and both pigments are allowed to emit characteristic fluorescence in addition to non-radiative EET. Energy transfer from Chl a resulting in formation of the $Chl^+/Pheo^-$ radical pair is also allowed to be reversible to account for the

possibility of charge recombination. ET from the radical pair to Q_a is assumed to be irreversible. Fluorescence emission bands were modeled as Gaussian bands with a full width at half maximum (FWHM) of 20 nm. The energy transfer from PBS to Chl a is associated with a characteristic time constant of around 100 ps (115 ps component, black curve in inset of Fig. 5B). The fluorescence exhibits an additional 160 ps component (red curve) associated with an ET from Chl a of PSII to pheophytin. The Chl a fluorescence decays biexponentially, since it is coupled to charge separation and charge stabilization and exhibits a small amplitude of a long decay component of 750 ps (green curve), accordingly. With the choice of the time constants as depicted in Fig. 5A, the simulated DAS for this model are shown in Fig. 5B. The agreement between experimental and simulated DAS (Fig. 5B, inset) is satisfactory assuming a typical intrinsic fluorescence decay of 1.3 ns for isolated PBSs and 2 ns for Chl a with an EET from PBS to Chl a with 130 ps (and 2 ns for the reverse transition). Values of 1.3 ns for PBS and 2 ns for Chl a might appear slightly faster than expected; however, they are in line with former studies and may vary slightly in the specific protein environment in *H. hongdechloris* (Petrasek et al. 2005). Charge separation should be around 160 ps with less than 10% recombination probability (2.5 ns), which is typical for open and active PSII RCs. The charge stabilization by ET to plastoquinone Q_a is assumed to occur with 700 ps to fit the experimental data. Thus, for WL-adapted cells, EET from PBS to the Chl a molecules in the RC results in charge separation, with a realistic set of intermediate states and rate constants.

To rationalize the situation in FRL-adapted cells, several reaction models were explored to account for the contribution of Chl f fluorescence in the observed DAS (Fig. 5C–H). In the first model (Fig. 5B, C), EET was allowed to occur all the way energetically downhill, first from PBS to Chl a, and from there in a reversible scheme to Chl f, from which charge separation and formation of the $Chl^+/Pheo^-$ radical pair should occur followed by subsequent ET to the Q_a site. The time constants of the components from the experimental DAS (inset in Fig. 5H) exhibit values of about 130–140 ps with a maximum in the fluorescence regime of APC (660 nm), 270 ps with maxima in the fluorescence regime of Chl a (680 nm) and Chl f (730 nm) and a long component with 1.1 ns which is solely observed at 730 nm (Chl f). The DAS simulated according to the scheme in Fig. 5C also show three components with very similar time constants (Fig. 5D). However, the amplitude relations between the simulated DAS components are distinctly different from the experimental DAS. In detail, with the assumption that charge separation occurs from Chl f, it is not possible to obtain large amplitudes of a long component ≥ 1 ns with maximum in the Chl f regime. Such a component can only be obtained within this scenario if one assumes an unreasonably long charge

Fig. 5 Comparison between experimental and simulated DAS to account for EET and ET processes in WL- (**A**, **B**) and FRL-adapted *H. hongdechloris* cells (**C**–**H**) upon excitation at 632 nm, according to the reaction schemes depicted in the left panels with time constants chosen for the simulations as indicated. For the situation in FRL-adapted cells, three different reaction schemes were explored to account for the possible involvement of Chl *f* in EET processes. Simulated DAS are shown on the right with Gaussian emission bands modeled with a FWHM of 20 nm, and the experimental DAS from Fig. 4 are shown for comparison in the insets. See text for details of the chosen reaction schemes
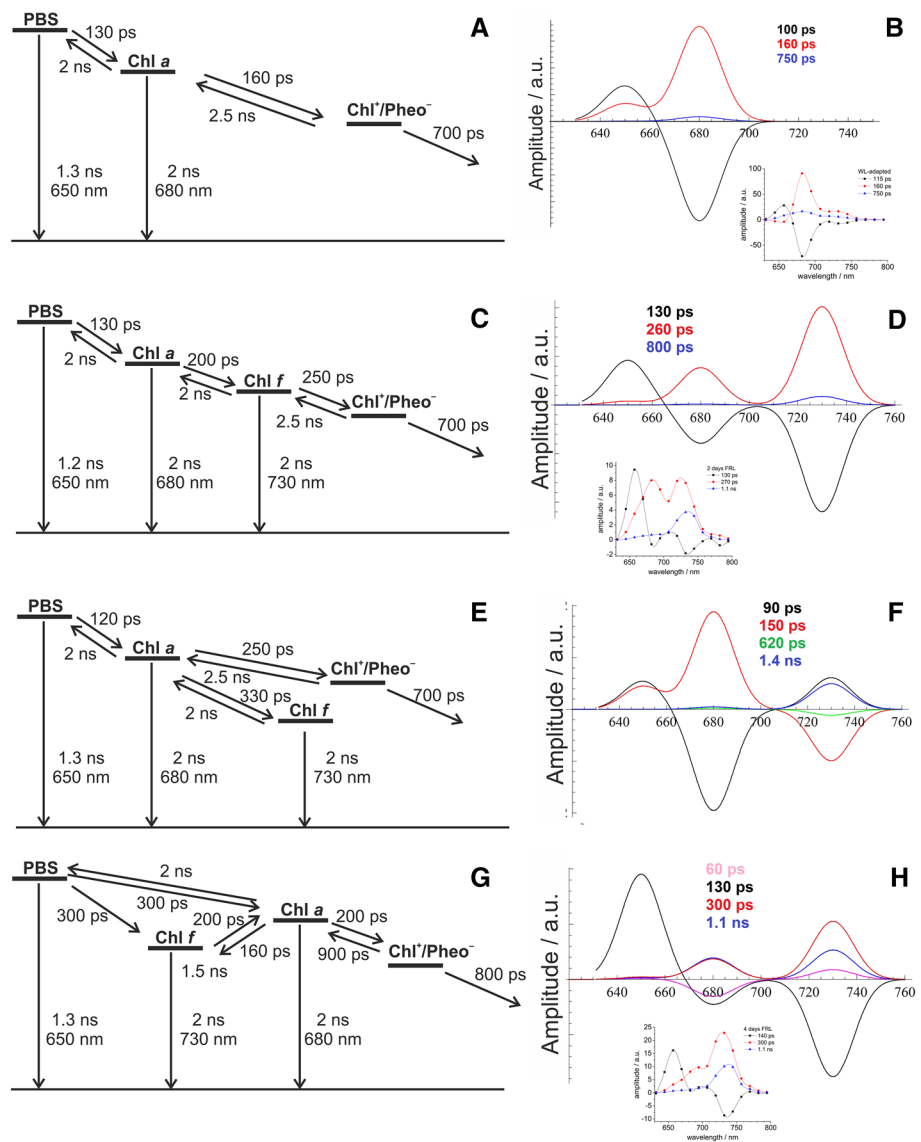
separation time with high recombination probability. However, such a situation is highly unlikely as it would not afford efficient ET to Q_a. Furthermore, the questions arises how the radical cation localized on Chl *f* would be able to provide a sufficient redox potential for water splitting. Therefore, compared to the measured DAS, the situation as depicted in Fig. 5C can be ruled out.

In the second model (Fig. 5E, F), Chl *f* was assumed to act as an isolated red-shifted energy trap, which is able to reversibly receive excitation energy from Chl *a* (which again primarily receives EET from PBS) in a dead-end side reaction, from which it would dissipate most of the excitation energy arriving on it. Charge separation was allowed to occur by radical pair formation from Chl *a* and subsequent ET to Q_a. Simulating the situation according to the reaction scheme with time constants as shown in Fig. 5E indeed reveals a decay component with long time constant (here:

1.4 ns) and high amplitude in the Chl *f* emission regime (730 nm). The time constant and amplitude of this component can be adjusted by choosing appropriate time constants for EET between Chl *a* and Chl *f*. However, in all cases, the negative amplitude (local minimum) of the very fast component in the experimental DAS (100 ps) is always found mainly at a wavelength of 680 nm (attributed to Chl *a*), because according to the scheme in Fig. 5E, EET occurs solely from PBS to Chl *a*. Since the measured DAS for the FRL-adapted samples exhibits a strong negative amplitude of the fast component (100 ps) in the region of Chl *f* emission (730 nm), it can be ruled out that the EET from PBS to Chl *a* is the only possible EET pathway.

In the third model (Fig. 5G, H), energy transfer from PBS was allowed to occur to Chl *a* and Chl *f* in parallel. Here, the transfer to Chl *f* was assumed to be essentially irreversible due to the large difference in energy levels, which should

make the reverse reaction highly improbable. In this model, we reasoned that the long excited state lifetime could endow Chl *f* with the ability to serve as an intermediary energy storage level in terms of a strongly coupled energy trap, from which it could transfer energy in an uphill process to Chl *a*, as it is considered for the well-known red Chl *a* species, in particular in PSI of higher plants (Croce et al. 2000). Our consideration takes into account the situation that Chl *f* (which maximally accumulates to about 10% of the total chlorophyll pool under FRL) is in energetic contact with a tenfold larger pool of Chl *a* molecules after the excited state localized on Chl *f* is thermally equilibrated. Thus, excitation energy arriving at Chl *f* sites is allowed to undergo uphill transfer to the Chl *a* pool, assuming a very short time constant of 200 ps only. Since the choice of this time constant is critical for the model to match experimental data, a thermodynamical justification is given in the Supplementary Information. In short, the factor of 10 in the size of the Chl *a* compared to the Chl *f* pool enlarges the entropy by $R \cdot \ln(10)$ per Mole (molar gas constant $R = 8.314$ J K^{-1}) during EET from Chl *f* to Chl *a*. Therefore, the Gibbs free energy of this process is reduced by $\Delta S \cdot T = +5.7$ kJ mol^{-1} at room temperature, which supports the uphill energy transfer by increasing the pre-exponential factor of the Arrhenius law (determined by the entropic term $\Delta S/R$ in the Eyring formulation of the Arrhenius activation energy) by a factor of about 10 (see Supplementary Information). The corresponding time constant for the EET from Chl *f* to Chl *a* directly reduces by the Chl *a*-to-Chl *f* ratio, and, therefore, is ten times smaller compared to the situation when equally sized pools of Chl *a* and Chl *f* are coupled. More detailed information about these thermodynamical considerations is found in the Supplementary Information.

In this sense, the 200 ps time constant is of the same order of magnitude as the one obtained for the Chl *a* to Chl *f* transfer from the fit of the experimental DAS. For the EET from Chl *a* towards formation of the radical pair, charge separation was also modeled with a time constant of 200 ps, with slightly higher recombination probability of 900 ps for the reverse process. Charge separation might proceed a bit slower, in accordance with slower charge stabilization (~ 800 ps) compared to WL-adapted cells (simulated in Fig. 5A). However, also in the present model, charge separation occurs from Chl *a* and would provide the redox potential necessary for water splitting. The EET and ET scheme as depicted in Fig. 5G yields a satisfactory fit of the experimental DAS with its characteristic EET from PBS directly to Chl *a* (686 nm), or directly to Chl *f* (730 nm) with 300 ps time constant for both EET pathways. The long ~ 1 ns component with high amplitude at 730 nm, as observed in the DAS, is well reproduced. The simulation also indicates that a further 60 ps component with small amplitudes is present, which was not resolved experimentally, since it is superseded by

the fast components with larger amplitude and the temporal width of the instrumental response function (IRF, 100 ps FWHM). Such fast components can only be resolved with specialized equipment that provides better time resolution than the multichannel TCSPC instrumentation used here. In summary, the reaction scheme depicted in Fig. 5G provides a minimal system of states and transitions, in which Chl *f* serves as an intermediary excitation energy trap that is directly excited from PBSs, and which is strongly coupled to a large pool of Chl *a* molecules. The sufficiently low Chl *f*-to-Chl *a* ratio ensures sufficient probability for EET to Chl *a*, all in good agreement with the observed DAS. If Chl *f* would reach higher levels of abundance, its contribution to EET to Chl *a* would possibly diminish dramatically, essentially as in the situation of the isolated trap model in Fig. 5E. Therefore, the low Chl *f*-to-Chl *a* ratio is possibly the result of optimization of light harvesting under FRL (730 nm), in spite of the fact that the overall absorbed amount of far-red light energy is proportional to the present amount of Chl *f*. It should be pointed out that there is no need to omit the degenerated states of Chl *a* in the model of Fig. 5E. However, in this case, the observed long lifetime in the Chl *f* regime (1.4 ns) deviates even more strongly from the measured decay times and the overall distribution of the lifetimes deviates more strongly from the observations compared to the presented model. Since the simulation does not reproduce the experimental features even when the degenerated states of Chl *a* in comparison to Chl *f* are introduced, the isolated antenna model as shown in Fig. 5E can be ruled out.

Anti-Stokes fluorescence detection

Fluorescence of an electronically excited molecule generally occurs red-shifted compared to the absorption spectrum. This is expressed as Stokes shift between the positions of the band maxima of absorption (excitation) and fluorescence emission as a result of vibrational relaxation and solvent reorganization (Lakowicz 2006). If the emitted photon has higher energy than the exciting one, the energy difference is termed an anti-Stokes shift. In solid state photonics, the gain in energy can stem from dissipation of thermal phonons in a crystal lattice, resulting in a process termed laser cooling (Clark et al. 1998). For fluorescent molecules in solution or embedded in biological matter, this process can occur by thermal activation, if the molecule to be excited is in a higher level than the vibrational ground state. The population of the vibrational states depends on the energy of the molecular vibration and the density of states in the excited vibrational state. As the vibrational state is given by combination of many vibrational modes in the case of polyatomic molecules as well as coupled modes between the probed molecules and the surrounding bath, the population probability rises with the degeneration factor of the

vibrational state in comparison to the ground state, which has to be multiplied with the probability expected from the band gap (Demtröder 2003). A molecular vibration with an energy of 1000 cm^{-1} (which is about the energy difference between 730 and 680-nm photons) corresponding to about 12 kJ mol^{-1}, which is almost five times $R \cdot T$ at 298 K, can, therefore, be significantly excited even at room temperature. However, anti-Stokes fluorescence is strongly temperature-dependent, freezing out at low temperatures, and the activation energy increases, the more blue-shifted to the excitation wavelength the phenomenon is intended to be measured.

To obtain further experimental evidence for the contribution of Chl f to photosynthesis in FRL-adapted *H. hongdechloris* cells, we directly tested for anti-Stokes fluorescence by exciting with a wavelength of (720 ± 10) nm to directly target Chl f and detection of blue-shifted fluorescence from Chl a species (680 ± 10) nm with a short wavelength bandpass filter. Results of such experiments are shown in Fig. 6.

Of note, anti-Stokes fluorescence upshifted by about 40 nm was even recorded from WL-adapted cells

(Fig. 6A), which may represent uphill energy transfer from the well-known red Chl a species to normal Chl a molecules in the RCs (Akimoto et al. 2015; Tomo et al. 2014). However, the signal amplitude was by an order of magnitude smaller than the robust blue-shifted fluorescence emission obtained from FRL-adapted cells (Fig. 6A, note the logarithmic scale for comparing the amplitudes). Blue-shifted fluorescence emission was enhanced in FRL-adapted cells upon addition of DCMU, indicating that a substantial part of the observed processes results from PSII activity. Such a DCMU effect was absent in WL-adapted cells indicating that such uphill energy transfer from red Chl a molecules might only occur in PSI (where more of those red-shifted molecules are present).

Figure 6B shows the result of anti-Stokes fluorescence experiments on FRL-adapted cells as in Fig. 6A carried out at different temperatures (5–30 °C). The integrals of the recorded fluorescence decay curves were plotted on a logarithmic scale against the reciprocal temperature, and the resulting Arrhenius plot was fitted by a straight line resulting
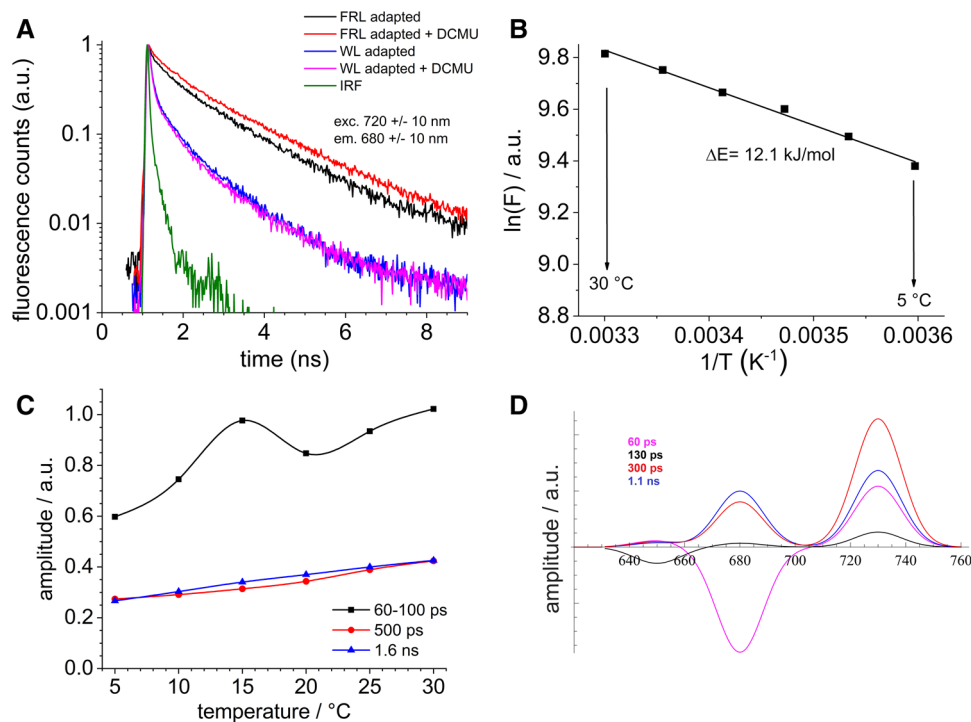

Fig. 6 Anti-Stokes fluorescence measurements on intact *H. hongdechloris* filament bundles adapted to WL or to FRL for 4 days. In **A** fluorescence was excited with a ps-pulsed laser at 720 ± 10 nm and a 680 ± 10 nm bandpass filter was used in the detection channel. WL-adapted cells were measured in presence (magenta curve) and absence (blue curve) of DCMU as well as FRL-adapted cells in presence (red curve) and absence (black curve) of DCMU. The green curve represents the instrumental response function (IRF) of the setup, as determined from measuring light scattering from the cyanobacterial colony directly in the spectrometer cuvette. **B** The result of anti-Stokes fluorescence experiments on FRL-adapted cells carried out at temperatures between 5 and 30 °C and plotted in form of the natural logarithm of the fluorescence signal F over 1/T. The linear fit of the data reveals an Arrhenius activation energy of 12.1 kJ mol^{-1}. **C** The time constants and amplitudes found in independent fits of the fluorescence decay curves measured on samples in absence of DCMU after FRL adaption for 4 days for different temperatures. Superimposed are cubic spline curves connecting the data points to guide the eye. **D** Resembles the expected result of a simulated DAS according to the coupling scheme presented in Fig. 5G if only Chl f (730 nm) is excited at $t = 0$

in an activation energy of 12.1 kJ mol^{-1}, which is well in line with the 40 nm gap between excitation and emission detection covered in the experiment.

The time-resolved fluorescence decay curves of the FRL-adapted cells in the absence of DCMU (Fig. 6A, black curve) monitored at 680 nm after excitation at 720 nm were subjected to fitting for all temperatures between 5 and 30 °C with linked parameters for the fluorescence decay time and three exponential components, which yielded sufficient fit quality. Three components with time constants of 50–100, 500 ps and 1.6 ns resulted from these fits (Fig. 6C). Interestingly, the amplitude of each component (with some variation for the fastest 50–100 ps component) increased with rising temperature following the Arrhenius equation with 12.5 ± 1.0 kJ mol^{-1} activation energy (data not shown) indicating that all three components are caused by anti-Stokes fluorescence from Chl a after excitation of Chl f. However, it was not possible to resolve a fluorescence rise kinetics as expected for fast EET from Chl f to Chl a.

To obtain deeper insight into this phenomenon, the coupling scheme as depicted in Fig. 5G was recalculated assuming direct excitation of Chl f instead of excitation of PBP as done for the simulation shown in Fig. 5H. The resulting simulated DAS are shown in Fig. 6D. Interestingly, there is no 200 ps rise kinetics observable at Chl a because the fast charge separation from Chl a with a similar time constant leads to fast positive fluorescence components that strongly change the expected time constants of the rise kinetics when the system of coupled linear differential equations is solved. The solution of the equation system indicates that a fluorescence rise kinetics of 60 ps is expected at Chl a according to the coupling scheme shown in Fig. 5G. However, 60 ps are difficult to resolve with the employed setup. In addition, it has to be pointed out that the excitation energy during 720 nm excitation was much higher (1000 W m^{-2}) than the physiological values during 632 nm excitation (10 W m^{-2}) to monitor the DAS and fluorescence decay curves shown in Fig. 4. For measuring anti-Stokes fluorescence, high excitation intensities are required to obtain sufficient signal amplitudes, which increases the probability for singlet–singlet annihilation, Pauli blocking (Richter et al. 2008), fast fluorescence components from PS I and stray light, which cannot be completely blocked by the applied laser filters (680 ± 10 nm bandpass and 720 ± 10 nm bandpass) interfere with the expected fluorescence rise kinetics and change the values of the obtained time constants. Therefore, the rise kinetics with 60 ps expected to be present in the Chl a regime according to the simulation shown in Fig. 6D cannot be resolved with the experimental setup used here.

In photosynthetic organisms from plants to algae and cyanobacteria, red Chl a species with absorption maxima up to 760 nm are known since many years. In eukaryotes, these are mostly located in LHCs, and their function in energy storage is under ongoing debate, since substantial uphill energy transfer to the Chl a special pair would be required (Chen and Blankenship 2011). These red Chl species are generally *not* considered to increase the rate of energy flow from antennae to the RCs. Rather, evidence from cyanobacterial core complexes and eukaryotic PSI-LHC systems suggests that the red forms retard energy flow to the RCs due to their role as an energy trap and slow energetically uphill energy transfer finally reaching the special pair (Jennings et al. 2003; Croce et al. 2000; Gobets et al. 2001; Trissl 1993). However, thermally activated energy transfer from red spectral states to bulk Chls in the PSI-LHC system from maize thylakoids was indeed observed as possible rate-limiting step for the charge separation (Croce et al. 2000), with activation energies between 7 and 13 kJ mol^{-1} complying with the Arrhenius-Eyring theory (Jennings et al. 2003). In an algal *Ostreobium* species, which can perform assimilation under light above 700 nm and is known for its high content of red Chl a molecules, direct evidence for uphill energy transfer from red Chls even to PSII was observed (Wilhelm and Jakob 2006), which is reasonable, since both photosystems must be able to operate in a balanced fashion under FRL to drive carbon fixation. Anti-Stokes fluorescence in chloroplasts can even be observed upshifted by more than 100 nm, as shown in a study operating with 800 nm excitation (Hasegawa et al. 2011). The obtained signals can even be utilized for discriminating between PSI and PSII in life-cell fluorescence imaging applications and for determination of the local temperature (Hasegawa et al. 2011).

Thus, the notion that a cyanobacterium utilizing Chl f when exclusively cultivated under FRL might not only operate PSI but also PSII by anti-Stokes excitation energy transfer resulting from electron–phonon interaction (of the excited electron with intramolecular vibrations) during the excited state lifetime of Chl f might not come as a surprise. Yet, the problem persists that PSII must provide the oxidation potential for water splitting, making it rather unlikely that Chl f is part of the P700 special pair. Indeed a recent study found that this is not the case (Li et al. 2018). The situation in *A. marina* employing Chl d might be different, since it is suggested that water oxidation occurs from a heterodimer formed from Chl a and Chl d (Schlodder et al. 2007). However, the main point is that the uphill energy transfer process in *H. hongdechloris* is apparently so efficient, because far-red illumination of FRL-adapted cells still leads to about 50% of the oxygen-evolving activity compared to WL illumination at the same intensity (Li et al. 2014). We have also performed simulations for the probability of charge separation based on the strongly coupled Chl f trap model as depicted in Fig. 5G (see Supplementary Fig. 3). Our simulations indicate that charge separation can achieve more than 50% yield as compared to WL-adapted samples, when Chl f in FRL-adapted samples is excited

at 720 nm. Such an efficient charge separation cannot be achieved, if the rate constant for the uphill energy transfer is determined by anti-Stokes fluorescence of equal pools of Chl *a* and Chl *f*, which are not supported by a gain in entropy during uphill EET from Chl *f* to Chl *a* (see Supplementary Fig. 3). Previous studies have already addressed the principal problem of uphill energy transfer by anti-Stokes processes in photosynthesis even on the level of thermodynamic theory (Jennings et al. 2003). We hope to contribute to this field elucidating further details about how nature might take advantage from an entropy effect that substantially speeds up EET rates while not changing the activation energies. Thus, it is our hope that this study will stimulate further investigations to scrutinize our hypothesis. The idea is based on the observation of a limited abundance of Chl *f* not exceeding more that 10% of the total Chl pool and suggests that EET rates are substantially speeded up, if each Chl *f* molecule on average is in EET contact to a tenfold larger Chl *a* pool. The conditions in the photosystems of *H. hongdechloris* are indeed favorable, as reported in the recent study of Li and coworkers, who purified and characterized photosystem preparations from WL- and FRL-adapted *H. hongdechloris* cells (Li et al. 2018). Sucrose density gradient centrifugation of detergent-solubilized thylakoid membranes yielded fractions enriched in PSI and PSII, and Chl *f* was only present in samples from FRL-adapted cells. Chl *f* reached about 8.4% of total chlorophyll content in the PSI- and 12% in the PSII-enriched fraction showing that Chl *f* is employed in both photosystems at a ratio of 1 to 8…12 (Li et al. 2018), which agrees with the considerations regarding the Chl pool sizes and the photosystem composition made herein. It is also in line with the previously proposed hypothesis (Ho et al. 2016) that the Chl *f*-binding PsbA4 protein (identified as Chl *f* synthase), which is dysfunctional in water oxidation but may associate with active RCs, may serve as light-harvesting antenna. The temperature-dependent anti-Stokes fluorescence from Chl *a* after excitation of Chl *f* shows that the time constants of the observed Chl *a* emission are independent from temperature, while the amplitudes of all fluorescence decay components follow the Arrhenius law with very similar activation energies. This effect can well be explained by a thermal activation of the EET from Chl *f* to Chl *a*, which can serve as a justification to simulate the obtained DAS using rate equation models for EET between all species.

To this end, we cannot exclude that different combinations of time constants could also explain the measured DAS. Furthermore, certain temperature-dependent changes of the probability values for photosynthetic processes might also interfere with the calculated DAS. Therefore, our results only put forward a consistent explanation of the observed data, but they cannot serve as a proof of the exact values of the various transfer rate constants. More complex models with increasing numbers of free parameters may result in different linear combinations of time constants that all allow for the simulation of the same fluorescence decay. Therefore, our simulation efforts should be considered to provide a "minimal model," as simple as possible, to rationalize experimental data.

Conclusions

The present study addresses the question whether Chl *f* in FRL-adapted *H. hongdechloris* cells can contribute to oxygenic photosynthesis. By using ps-to-ns time-resolved fluorescence spectroscopy on intact far-red light-adapted *H. hongdechloris* filament bundles at room temperature, we provide evidence that efficient charge separation in the Chl *a*-containing RC is possible after excitation of Chl *f* by far-red light due to an uphill excitation energy transfer driven by entropy, whereas a role of Chl *f* as far-red-shifted excitation energy trap can rather be ruled out. Since anti-Stokes fluorescence in FRL-adapted cells is enhanced by DCMU treatment, we suggest that Chl *f* in PSII is directly employed in photosynthetic energy harvesting.

We are aware of the possibility that the entropy-driven mechanism for uphill energy transfer from Chl *f* to Chl *a* proposed here may also apply for other and more general settings such as energy transfer from red Chl *a* species to ordinary Chl *a* molecules in RCs, or from red-shifted terminal emitters of phycobilisome antennae to more blue-shifted pigments, as long as the red-shifted species are in excitation energy transfer distance to an about one order of magnitude larger pool of more blue-shifted acceptor molecules. The bioenergetic concept of intermediate energy storage on a low-energy level with long intrinsic lifetime combined with entropically favored uphill energy transfer to a larger high-energy pool can be considered as one of the most admirable developments in the evolution of life, which on purpose could not have been engineered in a smarter way.

Compliance with ethical standards

Conflict of interest The authors declare that there are no conflicts of interest.

References

Akimoto S, Shinoda T, Chen M, Allakhverdiev SI, Tomo T (2015) Energy transfer in the chlorophyll f-containing cyanobacterium, Halomicronema hongdechloris, analyzed by time-resolved fluorescence spectroscopies. Photosynth Res 125(1–2):115–122. https://doi.org/10.1007/s11120-015-0091-3

Akutsu S, Fujinuma D, Furukawa H, Watanabe T, Ohnishi-Kameyama M, Ono H, Ohkubo S, Miyashita H, Kobayashi M (2011) Pigment analysis of a chlorophyll f-containing cyanobacterium strain KC1 isolated from Lake Biwa. Photomed Photobiol 33:35–40

Allakhverdiev SI, Tomo T, Shimada Y, Kindo H, Nagao R, Klimov VV, Mimuro M (2010) Redox potential of pheophytin a in photosystem II of two cyanobacteria having the different special pair chlorophylls. Proc Natl Acad Sci USA 107(8):3924–3929. https://doi.org/10.1073/pnas.0913460107

Allakhverdiev SI, Tsuchiya T, Watabe K, Kojima A, Los DA, Tomo T, Klimov VV, Mimuro M (2011) Redox potentials of primary electron acceptor quinone molecule (QA)- and conserved energetics of photosystem II in cyanobacteria with chlorophyll a and chlorophyll d. Proc Natl Acad Sci USA 108(19):8054–8058. https://doi.org/10.1073/pnas.1100173108

Allakhverdiev SI, Kreslavski VD, Zharmukhamedov SK, Voloshin RA, Korol'kova DV, Tomo T, Shen JR (2016) Chlorophylls d and f and their role in primary photosynthetic processes of cyanobacteria. Biochemistry 81(3):201–212. https://doi.org/10.1134/S0006297916030020

Chen M (2014) Chlorophyll modifications and their spectral extension in oxygenic photosynthesis. Annu Rev Biochem 83:317–340. https://doi.org/10.1146/annurev-biochem-072711-162943

Chen M, Blankenship RE (2011) Expanding the solar spectrum used by photosynthesis. Trends Plant Sci 16(8):427–431. https://doi.org/10.1016/j.tplants.2011.03.011

Chen M, Schliep M, Willows RD, Cai ZL, Neilan BA, Scheer H (2010) A red-shifted chlorophyll. Science 329(5997):1318–1319. https://doi.org/10.1126/science.1191127

Chen M, Li Y, Birch D, Willows RD (2012) A cyanobacterium that contains chlorophyll f–a red-absorbing photopigment. FEBS Lett 586(19):3249–3254. https://doi.org/10.1016/j.febslet.2012.06.045

Clark JL, Miller PF, Rumbles G (1998) Red edge photophysics of ethanolic rhodamine 101 and the observation of laser cooling in the condensed phase. J Phys Chem A 102(24):4428–4437. doi:https://doi.org/10.1021/jp980589c

Croce R, Dorra D, Holzwarth AR, Jennings RC (2000) Fluorescence decay and spectral evolution in intact photosystem I of higher plants. Biochemistry 39(21):6341–6348

Demtröder W (2003) Molekülphysik, Theoretische Grundlagen und Experimentelle Methoden. De Gruyter, Oldenburg

Gan F, Shen G, Bryant D (2015) Occurrence of far-red light photoacclimation (FaRLiP) in diverse cyanobacteria. Life 5(1):4

Gobets B, van Stokkum IH, Rogner M, Kruip J, Schlodder E, Karapetyan NV, Dekker JP, van Grondelle R (2001) Time-resolved fluorescence emission measurements of photosystem I particles of various cyanobacteria: a unified compartmental model. Biophys J 81(1):407–424. https://doi.org/10.1016/S0006-3495(01)75709-8

Hasegawa M, Yoshida T, Yabuta M, Terazima M, Kumazaki S (2011) Anti-Stokes fluorescence spectra of chloroplasts in Parachlorella kessleri and maize at room temperature as characterized by near-infrared continuous-wave laser fluorescence microscopy and absorption microscopy. J Phys Chem B 115(14):4184–4194. https://doi.org/10.1021/jp111306k

Ho M-Y, Shen G, Canniffe DP, Zhao C, Bryant DA (2016) Light-dependent chlorophyll f synthase is a highly divergent paralog of PsbA of photosystem II. Science. https://doi.org/10.1126/science.aaf9178

Holt AS (1966) Recently characterized chlorophylls. In: Vernon LP, Seely GR (eds) The chlorophylls. Academic Press, New York, pp 111–118

Itoh S, Ohno T, Noji T, Yamakawa H, Komatsu H, Wada K, Kobayashi M, Miyashita H (2015) Harvesting far-red light by chlorophyll f in photosystems I and II of unicellular cyanobacterium strain KC1. Plant Cell Physiol 56(10):2024–2034. https://doi.org/10.1093/pcp/pcv122

Jennings RC, Zucchelli G, Croce R, Garlaschi FM (2003) The photochemical trapping rate from red spectral states in PSI-LHCI is determined by thermal activation of energy transfer to bulk chlorophylls. Biochim Biophys Acta 1557(1–3):91–98

Lakowicz JR (2006) Principles of fluorescence spectroscopy, 3rd edn. Springer, New York

Larkum AW, Kuhl M (2005) Chlorophyll d: the puzzle resolved. Trends Plant Sci 10(8):355–357. https://doi.org/10.1016/j.tplants.2005.06.005

Li Y, Scales N, Blankenship RE, Willows RD, Chen M (2012) Extinction coefficient for red-shifted chlorophylls: chlorophyll d and chlorophyll f. Biochim Biophys Acta 1817(8):1292–1298. https://doi.org/10.1016/j.bbabio.2012.02.026

Li Y, Lin Y, Loughlin PC, Chen M (2014) Optimization and effects of different culture conditions on growth of Halomicronema hongdechloris—a filamentous cyanobacterium containing chlorophyll f. Front Plant Sci 5:67. https://doi.org/10.3389/fpls.2014.00067

Li Y, Lin Y, Garvey CJ, Birch D, Corkery RW, Loughlin PC, Scheer H, Willows RD, Chen M (2016) Characterization of red-shifted phycobilisomes isolated from the chlorophyll f-containing cyanobacterium Halomicronema hongdechloris. Biochim Biophys Acta 1857(1):107–114. https://doi.org/10.1016/j.bbabio.2015.10.009

Li Y, Vella N, Chen M (2018) Characterization of isolated photosystem I from Halomicronema hongdechloris, a chlorophyll f-producing cyanobacterium. Photosynthetica. https://doi.org/10.1007/s11099-018-0776-x

Majumder EL, Wolf BM, Liu H, Berg RH, Timlin JA, Chen M, Blankenship RE (2017) Subcellular pigment distribution is altered under far-red light acclimation in cyanobacteria that contain chlorophyll f. Photosynth Res 134(2):183–192. https://doi.org/10.1007/s11120-017-0428-1

Manning WM, Strain HH (1943) Chlorophyll D, a green pigment from red algae. J Biol Chem 151(1):1–19

Marquardt J, Senger H, Miyashita H, Miyachi S, Morschel E (1997) Isolation and characterization of biliprotein aggregates from *Acaryochloris marina*, a Prochloron-like prokaryote containing mainly chlorophyll d. FEBS Lett 410(2–3):428–432

Marquardt J, Morschel E, Rhiel E, Westermann M (2000) Ultrastructure of *Acaryochloris marina*, an oxyphotobacterium containing mainly chlorophyll d. Arch Microbiol 174(3):181–188

Mielke SP, Kiang NY, Blankenship RE, Gunner MR, Mauzerall D (2011) Efficiency of photosynthesis in a Chl d-utilizing cyanobacterium is comparable to or higher than that in Chl a-utilizing oxygenic species. Biochim Biophys Acta 1807(9):1231–1236. https://doi.org/10.1016/j.bbabio.2011.06.007

Mimuro M, Akimoto S, Yamazaki II, Miyashita H, Miyachi S (1999) Fluorescence properties of chlorophyll d-dominating prokaryotic alga, *Acaryochloris marina*: studies using time-resolved fluorescence spectroscopy on intact cells. Biochim Biophys Acta 1412(1):37–46

Mimuro M, Hirayama K, Uezono K, Miyashita H, Miyachi S (2000) Uphill energy transfer in a chlorophyll d-dominating oxygenic photosynthetic prokaryote, *Acaryochloris marina*. Biochim Biophys Acta 1456(1):27–34

Mimuro M, Akimoto S, Gotoh T, Yokono M, Akiyama M, Tsuchiya T, Miyashita H, Kobayashi M, Yamazaki I (2004) Identification of the primary electron donor in PS II of the Chl

d-dominated cyanobacterium *Acaryochloris marina*. FEBS Lett 556(1–3):95–98

Miyashita H, Ikemoto H, Kurano N, Adachi K, Chihara M, Miyachi S (1996) Chlorophyll d as a major pigment. Nature 383:402. https://doi.org/10.1038/383402a0

Niedzwiedzki DM, Liu H, Chen M, Blankenship RE (2014) Excited state properties of chlorophyll f in organic solvents at ambient and cryogenic temperatures. Photosynth Res 121(1):25–34. https://doi.org/10.1007/s11120-014-9981-z

Petrasek Z, Schmitt F-J, Theiss C, Huyer J, Chen M, Larkum A, Eichler HJ, Kemnitz K, Eckert H-J (2005) Excitation energy transfer from phycobiliprotein to chlorophyll d in intact cells of *Acaryochloris marina* studied by time- and wavelength-resolved fluorescence spectroscopy. Photochem Photobiol Sci 4(12):1016–1022. https://doi.org/10.1039/B512350J

Richter M, Renger T, Knorr A (2008) A Bloch equation approach to intensity dependent optical spectra of light harvesting complex II. Photosynth Res 95(2):119–127. https://doi.org/10.1007/s11120-007-9256-z

Schlodder E, Çetin M, Byrdin M, Terekhova IV, Karapetyan NV (2005) P700+- and 3P700-induced quenching of the fluorescence at 760 nm in trimeric photosystem I complexes from the cyanobacterium *Arthrospira platensis*. Biochimica et Biophysica Acta (BBA) 1706(1):53–67. https://doi.org/10.1016/j.bbabio.2004.08.009

Schlodder E, Cetin M, Eckert HJ, Schmitt FJ, Barber J, Telfer A (2007) Both chlorophylls a and d are essential for the photochemistry in photosystem II of the cyanobacteria, *Acaryochloris marina*. Biochim Biophys Acta 1767(6):589–595. https://doi.org/10.1016/j.bbabio.2007.02.018

Schmitt FJ (2011) Picobiophotonics for the investigation of pigment-pigment and pigment-protein interaction in photosynthetic complexes. Dissertation, Technical University of Berlin, Berlin

Schmitt F-J, Wache K, Fuesers J, Andree S, Handojo A, Karradt A, Kiekebusch D, Eichler H-J, Eckert H-J (2006) Investigation of the excited state dynamics in the Chl d-containing cyanobacterium *Acaryochloris marina* by time- and wavelength-correlated single photon counting. Proc SPIE 6386:638607. https://doi.org/10.1117/12.689127

Theiss C, Schmitt FJ, Pieper J, Nganou C, Grehn M, Vitali M, Olliges R, Eichler HJ, Eckert HJ (2011) Excitation energy transfer in intact cells and in the phycobiliprotein antennae of the chlorophyll d containing cyanobacterium *Acaryochloris marina*. J Plant Physiol 168(12):1473–1487. https://doi.org/10.1016/j.jplph.2011.02.002

Tomo T, Okubo T, Akimoto S, Yokono M, Miyashita H, Tsuchiya T, Noguchi T, Mimuro M (2007) Identification of the special pair of photosystem II in a chlorophyll d-dominated cyanobacterium. Proc Natl Acad Sci USA 104(17):7283–7288. https://doi.org/10.1073/pnas.0701847104

Tomo T, Allakhverdiev SI, Mimuro M (2011) Constitution and energetics of photosystem I and photosystem II in the chlorophyll d-dominated cyanobacterium *Acaryochloris marina*. J Photochem Photobiol B 104(1–2):333–340. https://doi.org/10.1016/j.jphotobiol.2011.02.017

Tomo T, Shinoda T, Chen M, Allakhverdiev SI, Akimoto S (2014) Energy transfer processes in chlorophyll f-containing cyanobacteria using time-resolved fluorescence spectroscopy on intact cells. Biochim Biophys Acta 1837(9):1484–1489. https://doi.org/10.1016/j.bbabio.2014.04.009

Trissl HW (1993) Long-wavelength absorbing antenna pigments and heterogeneous absorption bands concentrate excitons and increase absorption cross section. Photosynth Res 35(3):247–263. https://doi.org/10.1007/BF00016556

Wilhelm C, Jakob T (2006) Uphill energy transfer from long-wavelength absorbing chlorophylls to PS II in *Ostreobium* sp. is functional in carbon assimilation. Photosynth Res 87(3):323–329. https://doi.org/10.1007/s11120-005-9002-3

Willows RD, Li Y, Scheer H, Chen M (2013) Structure of chlorophyll f. Org Lett 15(7):1588–1590. https://doi.org/10.1021/ol400327j

Affiliations

Franz-Josef Schmitt[1] ⬤ · **Züleyha Yenice Campbell**[1] · **Mai Vi Bui**[1] · **Anne Hüls**[1] · **Tatsuya Tomo**[2] · **Min Chen**[3] · **Eugene G. Maksimov**[4] · **Suleyman I. Allakhverdiev**[5,6,7,8,9] ⬤ · **Thomas Friedrich**[1] ⬤

[1] Institute of Chemistry PC 14, Technical University of Berlin, Straße des 17. Juni 135, 10623 Berlin, Germany

[2] Department of Biology, Faculty of Science, Tokyo University of Science, Kagurazaka 1–3, Shinjuku-Ku, Tokyo 162-8601, Japan

[3] School of Life and Environmental Sciences, University of Sydney, Sydney, NSW 2006, Australia

[4] Department of Biophysics, Faculty of Biology, Lomonosov Moscow State University, Leninskye Gory 1, bld.24, Moscow, Russian Federation 119991

[5] Faculty of Biology, M.V. Lomonosov Moscow State University, Moscow, Russian Federation 119992

[6] Bionanotechnology Laboratory, Institute of Molecular Biology and Biotechnology, Azerbaijan National Academy of Sciences, Matbuat Avenue 2a, 1073 Baku, Azerbaijan

[7] Moscow Institute of Physics and Technology, Institutsky Lane 9, Dolgoprudny, Moscow Region, Russian Federation 141700

[8] Controlled Photobiosynthesis Laboratory, Institute of Plant Physiology, Russian Academy of Sciences, Botanicheskaya Street 35, Moscow, Russian Federation 127276

[9] Institute of Basic Biological Problems, Russian Academy of Sciences, Pushchino, Moscow Region, Russian Federation 142290